Bull. Disas. Prev. Res. Inst., Kyoto Univ., Vol. 22, Part 2, No. 202, February, 1973

# Internal Waves in Lake Biwa (II)
## ——Numerical experiments with a two layer model——

By Seiichi KANARI

(Received January 27, 1973)

**Abstract**

Surface and internal elevations and velocities in two layer Lake Biwa have been calculated numerically using a constant depth model with $25 \times 62$ square mesches of 1 km intervals. Linear hydrodynamic equations for the equivalent volume transports and the equivalent elevations were integrated by means of an implicit method, taking into account wind stress, bottom stress and Colioris force.

In the present experiment, the case of duration time of 450 minutes for a NW-wind of 5 m/sec and of interface position of 17.5 m at the equilibrium and density difference of $2.5 \times 10^{-3}$ g/cm$^3$ between upper and lower layers was treated.

From the results of Fourier spectrum analysis for the calculated time series of elevation and velocity at various sampling positions in the model lake, the long period internal Kelvin waves and internal Poincare waves were distinguished.

## 1. Introduction

The problem of the current pattern and of lake water oscillation under geostrophic effect is one of the most important topics in recent physical limnology, because the rotation of the earth affects the movements of lake water, especially in the large scale lakes which are always playing the important role of a natural reservoir. Consequently, from the stand point of water quality control or prevention of water pollution of lakes, these effects can never be ignored.

However, up to the present day, there are many points concerning the large scale motions in the stratified lake under geostrophic effects, which have not been solved.

This situation is also true of Lake Biwa. From the time series analysis of a large number of temperature records which were obtained during the period from summer to late autumn, two or three day periods internal oscillations and other higher harmonics can be often found in Lake Biwa. The analyzed period of order of two or three days often has agreed with the period calculated as a longitudinal oscillation in a two layer lake by using the Merians formula in the case of no rotation[1]. It seemed that there was no trouble apparently about such a long period internal oscillation whose existence was confirmed recently.

It is not reasonable, however, that such a large scale motion of the long period can be free from the Colioris effect. Another difficulty was found from an observation at Funaki-saki, situated midway along the western shore of the north basin. If we consider the long period internal oscillation as the longitudinal one without any rotation, the node must be found at Funaki-saki. From the result of the observation, unfortunately, the considerably large amplitude oscillation of the long period, which is comparable with those found at the north or the south end of the north basin,

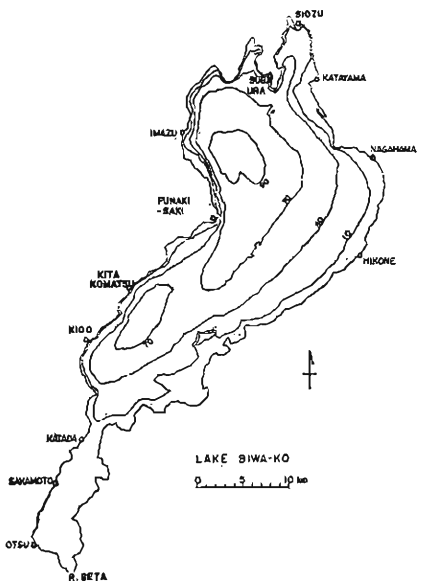


Fig. 1. Bathymetric map of Lake Biwa (in meters).

were also found at Funaki-saki. Then, it was considered that the observed result might be suggesting the rotating internal waves. G. T. Csanady[2] and G. E. Birchfield[3] have treated theoretically a large scale motions in the Great Lake as a simple two-layered rotating circular basin using linear equations of motion, and clarified the natures of the long period internal Kelvin waves and the median period Poincare waves in the Great Lake.

In the present model lake the complicated feature of the shore line of the real lake was taken into account. Accordingly, in consequence of the complicated boundary, it is difficult to obtain the theoretical prospects, but the numerical method enables us to obtain some realistic behavior of water movements. In such a situation, the numerical model experiments of the two layer Lake Biwa (35°N, 136°E) were performed, using the constant depth model (north basin, 50 m; south basin, 5 m) with $25 \times 62$ square meshes of 1 km intervals, in which the direction of $j$-axis is toward N 26°30′E and i-axis is toward E26°30′S as shown in Fig. 2. Of course, the numerical integration of the equations of motion by means of implicit method may be unsuitable to give the prospects of the analogous phenomena, but it will be convenient when comparing the results of numerical experiment with the results of observation.

## 2. Equations of motion

The present paper deals comparatively large scale and long period motions of the period greater than 2 hours (this limit is due to a sampling interval of the calculated time series). The only exception can be seen in the treatment concerning the response of the surface elevation to the wind action. In this case, though, the lengths of the studying time seriesare less than 15 hours, a sampling was made every 10 minutes.

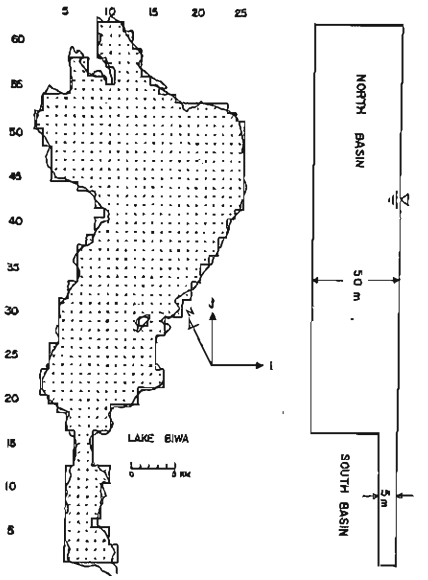


Fig. 2. Computational grid and longitudinal cross-section of model Lake Biwa.

If we ignore the inertial nonlinear terms in the equations of motion and define vertically integrated volume transport vector in both upper and lower layers, then the equations of motion and the equation of continuity can be written as follows;

$$\begin{cases} \dfrac{\partial U_1}{\partial t} - fV_1 = -g(h_1+\zeta_1-\zeta_2)\dfrac{\partial \zeta_1}{\partial x} + \dfrac{1}{\rho_1}(\tau_{sx}-\tau_{ix}) \\ \dfrac{\partial V_1}{\partial t} + fU_1 = -g(h_1+\zeta_1-\zeta_2)\dfrac{\partial \zeta_1}{\partial y} + \dfrac{1}{\rho_1}(\tau_{sy}-\tau_{jy}) \\ \dfrac{\partial \zeta_1}{\partial t} = \dfrac{\partial \zeta_2}{\partial t} - \left(\dfrac{\partial U_1}{\partial x} + \dfrac{\partial V_1}{\partial y}\right) \end{cases} \quad \cdots\cdots (1)$$

$$\begin{cases} \dfrac{\partial U_2}{\partial t} - fV_2 = -\dfrac{\rho_1}{\rho_2}\left[g(h_2+\zeta_2)\dfrac{\partial \zeta_2}{\partial x} + \dfrac{\Delta\rho}{\rho_1}\cdot\dfrac{\partial \zeta_2}{\partial x}\right] + \dfrac{1}{\rho_2}(\tau_{ix}-\tau_{bx}) \\ \dfrac{\partial V_2}{\partial t} + fU_2 = -\dfrac{\rho_1}{\rho_2}\left[g(h_2+\zeta_2)\dfrac{\partial \zeta_2}{\partial y} + \dfrac{\Delta\rho}{\rho_1}\cdot\dfrac{\partial \zeta_2}{\partial x}\right] + \dfrac{1}{\rho_2}(\tau_{iy}-\tau_{by}) \\ \dfrac{\partial \zeta_2}{\partial t} = -\left(\dfrac{\partial U_2}{\partial x} + \dfrac{\partial V_2}{\partial y}\right) \end{cases} \quad \cdots (2)$$

where $U_1$, $U_2$, etc. denote the horizontal volume transport in the respective layers defined by

$$U_1 = \int_{-\zeta_1}^{h_1} u_1 dz, \qquad U_2 = \int_{h_1-\zeta_2}^{h_2} u_2 dz, \quad \text{etc.} \qquad \cdots\cdots (3)$$

and $f$ is Colioris parameter, $\tau_s$, $\tau_i$ and $\tau_b$ are surface, interface, and bottom stresses respectively. The subindex 1 and 2 show the quantity referred to its respective layer. $\Delta\rho$ $(=\rho_2-\rho_1)$ is density difference between the upper and the lower layer respectively.

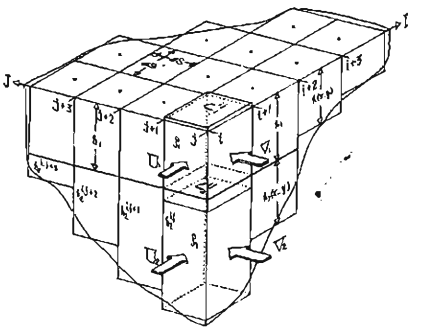

Fig. 3. Definition sketch of constants and computational variables referred to cross-sectional two layer columns.

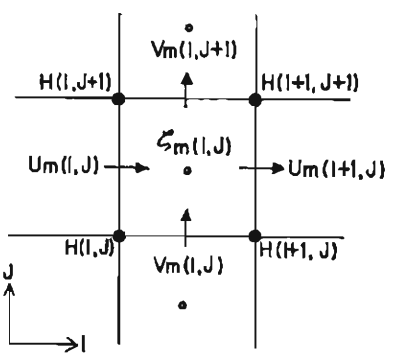


Fig. 4. Computational grid employed in model Lake Biwa. Black circles denote depth points; open circles indicate elevation points. Arrows indicate flow points.

Of course, in the derivation of equations (1) and (2), the nonlinear terms of elevations were neglected assuming that the surface elevation $\zeta_1$ and the interface elevation $\zeta_2$ are both small compared with the depths $h_1$ and $h_2$ of the respective layer and that the pressure field is hydrostatic.

Definitions of the variables used in eqs. (1) and (2) are illustrated in Fig. 3, even though the illustration was provided for the future model of variable depth.

The equations of (1) and (2) cannot be independent, because of the coupling through the surface and the interface elevation, $\zeta_1$ and $\zeta_2$. According to Veronis[4] and also Charney,[5] however, these two sets of equations can be transformed into two independent sets of equations by assuming the barotropic and baroclinic variables in the upper and the lower layer, that is

$$\begin{cases} U_m=\alpha_m U_1+U_2 \\ V_m=\alpha_m V_1+V_2 \\ \zeta_m=\alpha'_m\zeta_1+\beta'_m\zeta_2 \end{cases} \quad \cdots\cdots (4)$$

where $\alpha_m$, $\alpha'_m$, and $\beta'_m$ are constant coefficients of linear combination of variables for barotropic mode ($m\rightarrow s$) and baroclinic mode ($m\rightarrow i$) respectively.

The three coefficients can be determined by transformation of six variables $U_1$, $V_1$, $U_2$, $V_2$, $\zeta_1$, $\zeta_2$ into the new variables $U_m$, $V_m$, $\zeta_m$, using the equations (1), (2), (4), and then comparing each term of the new equations with those of the following equations for barotropic and baroclinic modes.

$$\begin{cases} \dfrac{\partial U_m}{\partial t}-fV_m=-C_m^2\dfrac{\partial \zeta_m}{\partial x}+F_{mx} \\ \dfrac{\partial V_m}{\partial t}+fU_m=-C_m^2\dfrac{\partial \zeta_m}{\partial y}+F_{my} \\ \dfrac{\partial \zeta_m}{\partial t}+\dfrac{\partial U_m}{\partial x}+\dfrac{\partial V_m}{\partial y}=0 \end{cases} \quad \cdots\cdots (5).$$

The equivalent wave velocity $C_m$ in the equation (5) can be determined as the roots of the Stokes equation which is obtained by the coefficient determining equation,

$$C_m^4-g(h_1+h_2)C_m^2+\frac{\Delta\rho}{\rho}g^2h_1h_2=0 \quad \cdots\cdots (6).$$

Then, neglecting the terms of $0((\Delta\rho)^2)$, the determined coefficients and the wave velocity can be written as follows;

$$\begin{cases} \alpha_s=\alpha'_s=1-\Delta\rho h_2/\rho(h_1+h_2) \\ \beta'_s=\Delta\rho h_2/\rho(h_1+h_2) \\ C_s=\sqrt{g(h_1+h_2)} \end{cases} \quad \cdots\cdots (7),$$

and

$$\begin{cases} \alpha_i=\alpha'_i=-h_2/h_1 \\ \beta'_i=1+h_2/h_1 \\ C_i=\sqrt{\Delta\rho\, g h_1h_2/\rho_2(h_1+h_2)} \end{cases} \quad \cdots\cdots (8).$$

$$\begin{cases} F_{sx}=\dfrac{1}{\rho_1}\left(1-\dfrac{\Delta\rho}{\rho_2}\cdot\dfrac{h_2}{(h_1+h_2)}\right),(\tau_{sx}-\tau_{ix})+\dfrac{1}{\rho_2}(\tau_{ix}-\tau_{sx}) \\ F_{sy}=\dfrac{1}{\rho_1}\left(1-\dfrac{\Delta\rho}{\rho_2}\cdot\dfrac{h_2}{(h_1+h_2)}\right)(\tau_{sy}-\tau_{iy})+\dfrac{1}{\rho_2}(\tau_{iy}-\tau_{by}) \end{cases} \quad \cdots\cdots (9)$$

$$\begin{cases} F_{ix}=-\dfrac{1}{\rho_1}\left(\dfrac{h_2}{h_1}\right)(\tau_{sx}-\tau_{ix})+\dfrac{1}{\rho_2}(\tau_{ix}-\tau_{bx}) \\ F_{iy}=-\dfrac{1}{\rho_1}\left(\dfrac{h_2}{h_1}\right)(\tau_{sy}-\tau_{iy})+\dfrac{1}{\rho_2}(\tau_{iy}-\tau_{by}) \end{cases} \quad \cdots\cdots (10)$$

where $\tau_{sx}$, $\tau_{ix}$, $\tau_{bx}$ denote $x$-components of surface wind stress, interface stress, and bottom stress respectively.

The equation (5) takes the same form for two modes, therefore, we can treat these modes independently as a two-dimensional equation for the entire body of lake water, and as will be mentioned later, calculation of the two modes was carried out with different time increments.

## 3. Initial and boundary conditions.

Surface seiches and internal seiches in Lake Biwa are mainly induced by wind stress blowing over the lake surface. Unfortunately, there are few meteolological stations around the lake shore, not to mention over the lake surface, so the distribution of wind stress over the lake surface is not certain. Therefore, it was assumed that the constant wind stress suddenly acts on the model lake, which has initially no motion.

As it is usually stated, it was assumed that wind stress, $\tau_s$ is proportional to the square of wind velocity;

$$\tau_s=\rho_a\gamma_a^2 W|W| \quad \cdots\cdots (11)$$

where, $\rho_a$ is density of air, and $\gamma_a^2$ is the drag coefficient, and $W$ is the wind velocity vector. Until recently, it has been supposed that the stress coefficient, $\gamma_a^2$ varies with the wind velocity[6], however, it will be assumed that the coefficient takes the constant value of $2.6\times10^{-3}$ in the present model, which may be slight over-estimation for the wind velocity of 5 m/sec.

In this paper, as mentioned above, a comparatively slow motion of the period longer than 2 hrs or so will be treated. For such a motion, the interface must be stable, because a sharp thermocline is kept for long periods in early autumn in Lake Biwa. Consequently, we assume the stress of interface, $\tau_i$ to be negligible.

Though there is no reasonable expression for the bottom stress, and only a few examples were found in the numerical experiments of storm surge, Reid[7], and also Miyazaki[8] proposed an expression for the bottom stress in the following form,

$$\tau_b=\rho_w\gamma_w^2 V|V|-\beta\tau_s \quad \cdots\cdots (12)$$

where, $\beta$ is some constant and it takes the value of $5\gamma_w^2$ in Reid's formula, and $\gamma_w^2$

is the coefficient of bottom stress. In a recent study, Nakano[9] showed the bottom stress of the seiche motion in lakes, is just proportional to the flow velocity, and the proportionality explains reasonably the decay of the amplitude of surface oscillation.

Then, we also assumed the linear relationship for the bottom stress, that is

$$\tau_b = \rho_w K_w U - \beta \tau_s \qquad \cdots\cdots (13)$$

where, $K_w$ is a constant coefficient of the same dimension as that of flow velocity, and $U$ denotes the flow vector. In the present paper, we may take the value of $\beta$ to be 1.0 and of $K_w$ to be $2.6 \times 10^{-2}$ (cm/sec), which corresponds to the bottom stress in the case of the flow velocity of 1 cm/sec in (12).

The flow velocity normal to the shore line must vanish at the shore. Consequently, it leads to the following boundary condition;

$$\boldsymbol{V} \cdot \boldsymbol{n} = 0 \qquad \cdots\cdots (14),$$

where $\boldsymbol{n}$ is a unit vector normal to the shore line.

## 4. Difference equations.

As illustrated in Figs. 3 and 4, the mesh point of flow calculation is in the center of the two adjacent depth points which have the mesh interval of 1 km, and the mesh point of elevation calculation is in the center of the four depth points. Therefore, the mesh interval between flow and elevation is $\Delta s/2$. In addition, the calculations of flow and elevation are carried out alternately with the time increment of $\Delta t$ respectively. Hence, the time step of the calculation for successive flow and elevation is $\Delta t/2$.

Then, we can write the difference equations of equation (5) in the form of prediction equations of flow and elevation at the point $(i, j)$ at every time increment $\Delta t_m$, i.e.,

$$\begin{cases} U_m^{i,j}(t_m+\Delta t_m) = U_m^{i,j}(t_m) - \lambda_m^{i,j}\{\zeta_m^{i+1,j}(t_m+\Delta t_m/2) - \zeta_m^{i,j}(t_m+\Delta t_m/2)\} \\ \qquad\qquad + \{fV_m^{i,j}(t_m) + F_{mx}^{i,j}(t_m)\}\Delta t_m \\ V_m^{i,j}(t_m+\Delta t_m) = V_m^{i,j}(t_m) - \lambda_m^{i,j}\{\zeta_m^{i,j+1}(t_m+\Delta t_m/2) - \zeta_m^{i,j}(t_m+\Delta t_m/2)\} \\ \qquad\qquad - \{fU_m^{i,j}(t_m) - F_{my}^{i,j}(t_m)\}\Delta t_m \qquad \cdots\cdots (15) \\ \zeta_m^{i,j}(t_m+\Delta t_m) = \zeta_m^{i,j}(t_m) - (\Delta t_m/\Delta_s)\{U_m^{i+1,j}(t_m+\Delta t_m/2) - U_m^{i,j}(t_m+\Delta t_m/2) \\ \qquad\qquad + V_m^{i,j+1}(t_m+\Delta t_m/2) - V_m^{i,j}(t_m+\Delta t_m/2)\} \end{cases}$$

where,

$$\lambda_m^{i,j} = (\Delta t_m/\Delta s)^2 (C_m^{i,j})^2 \qquad \cdots\cdots (16)$$

and $(C_m^{i,j})^2$, $F_{mx}^{i,j}$, $F_{my}^{i,j}$ are given by the following formulas according to the modal index $m$.

$$\begin{cases} (C_m^{i,j})^2_{m=s} = g\bar{H} \\ (C_m^{i,j})^2_{m=i} = \Delta\rho g h_1(\bar{H}-h_1)/\rho_2\bar{H} \\ \bar{H} = (H_{i,j}+H_{i+1,j}+H_{i+1,j+1}+H_{i,j+1})/4 \end{cases} \quad \cdots\cdots (17)$$

$$\begin{cases} \begin{pmatrix} F_{mx}^{i,j} \\ F_{my}^{i,j} \end{pmatrix}_{m=s} = \frac{\rho_a}{\rho_1}(1+\beta)\gamma_a^2 W|W| \cdot \begin{pmatrix} \cos\theta \\ \sin\theta \end{pmatrix} - \bar{\rho} K_w \begin{pmatrix} \sigma^{i,j+1} \cdot U_m^{i,j}(t_m) \\ \sigma^{i+1,j} V_m^{i,j}(t_m) \end{pmatrix}_{m=1} \\ \begin{pmatrix} F_{mx}^{i,j} \\ F_{my}^{i,j} \end{pmatrix}_{m=i} = \frac{\rho_a}{\rho_2}\left(1+\beta-\frac{\bar{H}}{h_1}\right)\gamma_a^2 W|W| \cdot \begin{pmatrix} \cos\theta \\ \sin\theta \end{pmatrix} \\ \qquad - \bar{\rho} K_w \cdot \begin{pmatrix} \sigma^{i,j+1} \cdot U_m^{i,j}(t_m) \\ \sigma^{i+1,j} \cdot V_m^{i,j}(t_m) \end{pmatrix}_{m=i} \\ \begin{pmatrix} \sigma^{i+1,j} \\ \sigma^{i+1,j} \end{pmatrix} = \begin{pmatrix} 2/(H_{i,j}+H_{i,j+1}) \\ 2/(H_{i,j}+H_{i+1,j}) \end{pmatrix} \end{cases} \quad \cdots\cdots (18)$$

It is to be noted that in the region of one layer, $h_1$ in equations (17) and (18) should be replaced by $\bar{H}$.

## 5. Stability of calculation.

In calculation of the difference equations (17), the validity of results may be destroyed by numerical instability induced by wrong selection of the value of time interval $\Delta t_m$.

The problems on the numerical instability have been discussed by Courant, Friedrichs, and Lewy (1965), Courant and Hilbert (1937), Kasahara (1965), and Fisher (1965). However, we do not intend to introduce a detailed discussion here.

According to the theory of numerical stability discussed by Courant-Friedrichs-Lewy, the stability criteria for a hyperbolic-type difference wave equation in the case of one layer is given by

$$\frac{\Delta t}{\Delta s} \leq \frac{1}{C} \quad \cdots\cdots (19),$$

where, $C$ is a propagation velocity of waves in the original wave equation[11]. And in general, in the case of $n$-dimensional space, the condition (19) can be written as follows[10];

$$\frac{\Delta t}{\Delta s} \leq \frac{1}{\sqrt{n}\, C} \quad \cdots\cdots (20).$$

Consequently, from (7) and (8), the expressions for the calculating time intervals of the barotropic and the baroclinic modes may be given by the following formulas

respectively,

$$\Delta t_s = \frac{\Delta s}{\sqrt{2}C_s} = \Delta s / \sqrt{2g \cdot H_{max}} \qquad \cdots\cdots (21)$$

$$\Delta t_i = \frac{\Delta s}{\sqrt{2}C_i} = \Delta s \sqrt{\rho_2 (H_{max}) / (2\Delta\rho g h_1 h_{2max})} \qquad \cdots\cdots (22)$$

where, $\Delta\rho$ is $2\times10^{-3}$ (g/cm$^3$), $h_1$ and $h_{2max}$ are 17.5 m and 32.5 m, respectively, and $H_{max}=h_1+h_{2max}$ in this case. Since the value of $\Delta s$ has already been set at 1 km, the stability criterions for the two modes become $\Delta t_s \leq 30$ sec and $\Delta t_i \leq 1600$ sec. However, for safety's sake, they were chosen to be

$$\Delta t_s = 20 \text{ sec.}$$

$$\Delta t_i = 1200 \text{ sec.}$$

## 6. Numerical results and analysis.

In the process of numerical calculation, the inversely transformed flow patterns in the both layers and elevations of surface and interface at all mesh points were printed out with the time interval of 15 minutes. At the same time, the flow velocities and flow directions in both layers, the elevations of surface and interface at ten sampling points were punched out with the time interval of 45 minutes as the input data for the time series analysis. Such a rough sampling interval of 45 minutes is based on the limitation of capacity of data processing. However, as will be mentioned later, it causes a wrong spectral component for short period surface seiches.

### (a) Variation of elevation and velocity.

Some examples of the variation of the elevation and velocity components at some typical sampling points are shown in Fig. 5 (1) and Fig. 5 (2). In these figures, the upper curve shows the variations of interface elevation, the middle shows the variation of surface elevation, and the lower one shows the variations of the velocity components in both layers (the numerals 1, 2, 3, and 4 correspond to the velocity components of $u_1$, $v_1$, $u_2$, and $v_2$ respectively).

As mentioned above, the time interval of the curve plotting is 45 minutes, therefore, short period changes of less than 90 minutes are uncertain. Jigging change in the surface elevation also may be due to the comparatively long sampling intervals.

More detailed change of the surface elevation at the typical mesh points of (8, 56), (4, 24), (10, 40), (20, 38), and (8, 2) are shown in Fig. 6. Under the surface condition of NW-wind of 5 m/sec, setup of the new equilibrium water surface seems to be accomplished about 1.2 hrs (about one-fourth of the prevailing period) after wind has risen. During the wind blow, the water surface is oscillating around the tilted equilibrium surface, but after the wind ceases, it oscillates freely as surface seiches around the horizontal equilibrium surface.

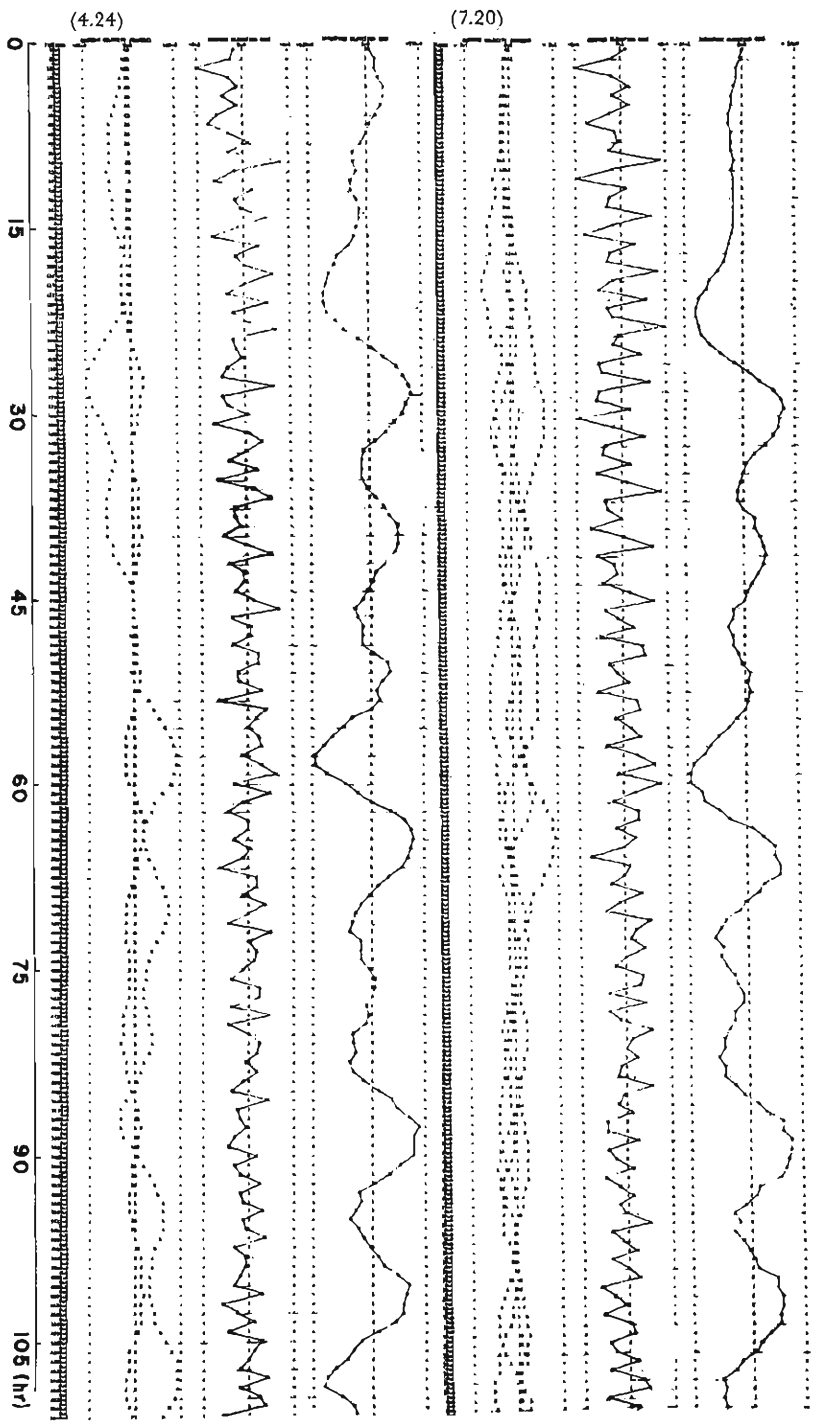


Fig. 5 (1). Calculated time serieses of interface elevation (upper), surface elevation (middle), and velocity components in both layers (lower) at the sampling points of (4, 24) and (7, 20).

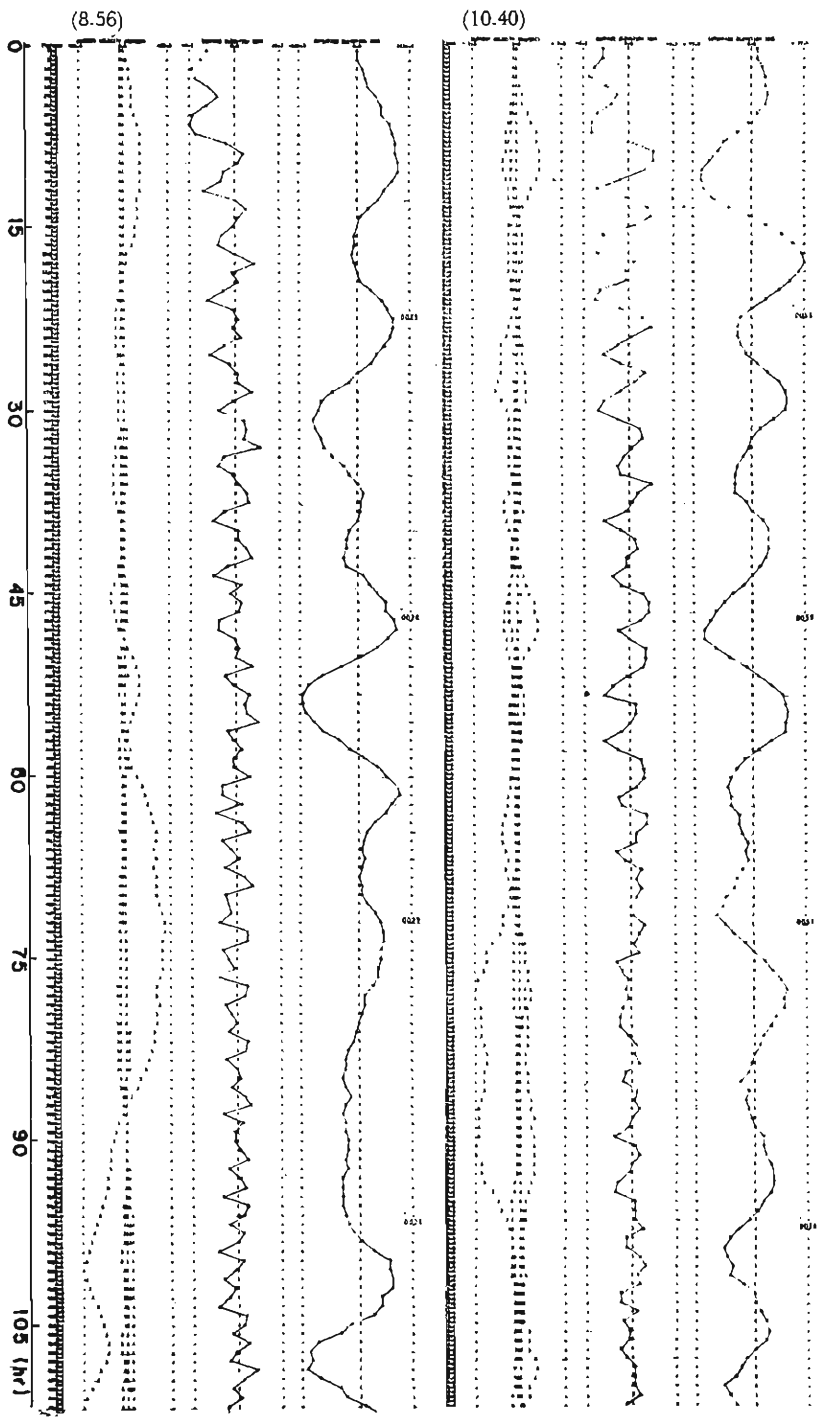


Fig. 5 (2). Calculated time serieses of interface elevation (upper), surface elevation (middle), and velocity components in both layers (lower) at the sampling points of (8, 56) and (10, 40).

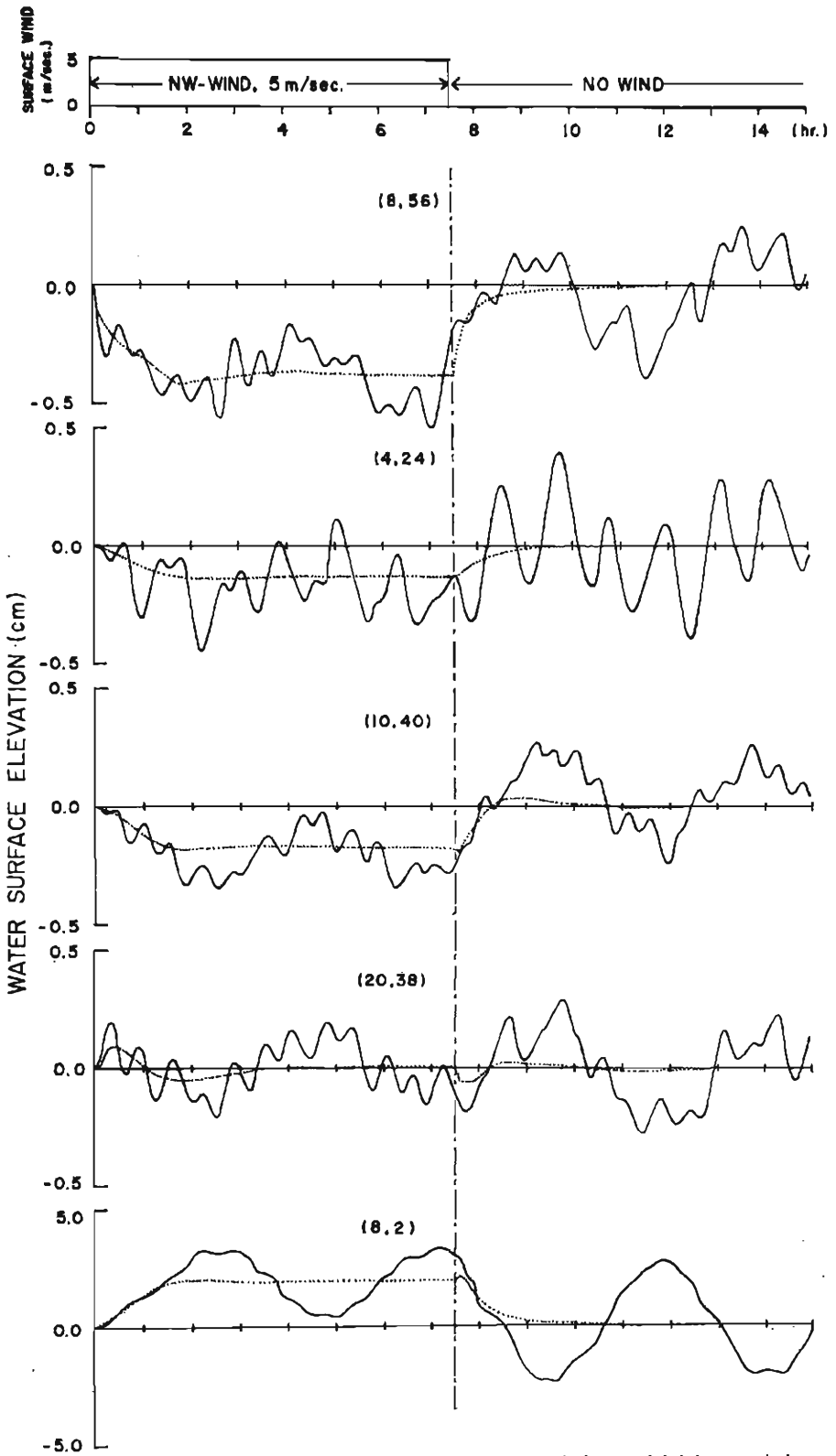


Fig. 6. Water surface response at various sampling points of the model lake to wind stress shown in the top of the same figure. The dotted line showing a quasistatic lake surface.

(b) Surface and interface configurations.

The water surface configurations at the stage of surface setup are shown in Fig. 7(1), and also the configurations at the stage of surface setback are shown in Fig. 7(2). From these figures it seems that the surface oscillation is prevailing in the longitudinal direction of the entire basin, and the maximum amplitude may appear in the south end of the south basin of the model lake.

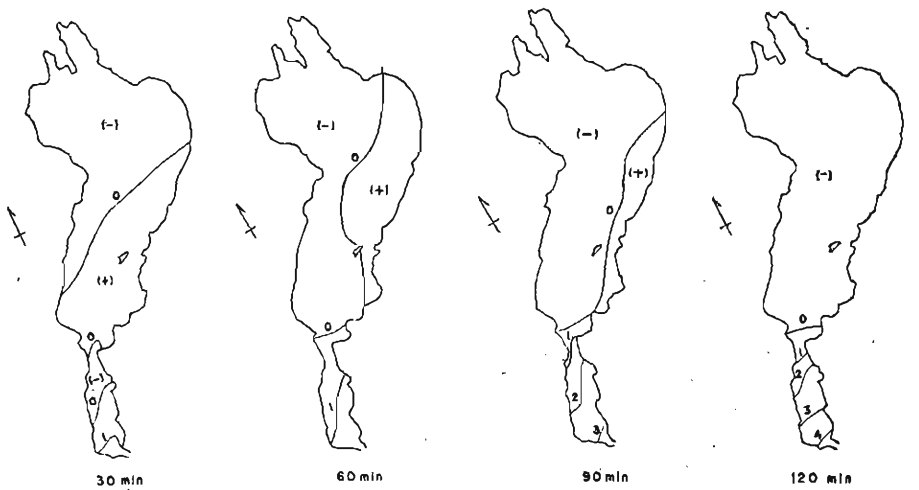


Fig. 7 (1). Spatial elevation patterns (in centi meters) of the model lake surface during wind blow.

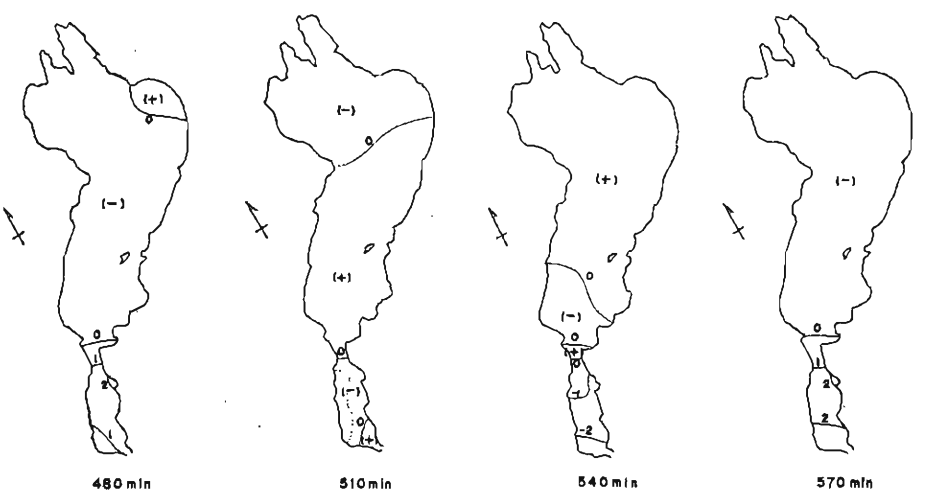


Fig. 7 (2). Spatial elevation patterns (in centi meter) of the model lake surface after blowing down of wind.

In the north basin, the node of the tilted equilibrium surface lies on the line of $j=38$, therefore, the tilt of the equilibrium surface in the north basin is 0.4 cm/20 km.

Fig. 8 shows the interface configuration at the time interval of 240 minutes. In this stage of the surface setup, the interface elevation is in contradiction to the surface elevation pattern in north basin, though its magnitude is more than several hundreds times of the surface elevation. After the ceasation of wind, however, the interface configuration takes a more complicated pattern as if it has no connection with the surface configuration. The apparently confused pattern will be made clear by Fourier analysis as will be mentioned latter.

(c) Power spectra .

At every sampling point, the Fourier power spectra and phase differences were estimated for the calculated time series of the surface and interface elevations in the stage of free oscillation. Some examples of the estimated power spectra are shown in Fig. 9 and Fig. 10. In these spectra of the surface elevation, Fig. 9 (3) shows the spectrum of surface seiches at the point of (10, 3) in the south basin, and the others show that in the north basin. It must be noted that the seiche motion with the period of 4.5 hrs is prevailing through the entire basin, while another one with the period of 2.2 hrs exists in the north basin only. A small fraction of the internal components are also appeared in the range of longer period.

In the spectra of the interface elevation as shown in Fig. 10, remarkable peaks appeared at the periods of 18.1 hrs and 12.7 hrs, and other smaller peaks appeared at the periods of 31.7 hrs and 63.4 hrs.

Now, we will examine some behaviors of oscillatory motions using the results of Fourier analysis. The $n$-th Fourier component at a sampling point, $(i, j)$ can be expressed by

$$\zeta_n(i, j, t)=\zeta_{0n}(i, j)\cos(\varphi_n-\omega_n t) \qquad \cdots\cdots\cdots\cdots\cdots\cdots (23).$$

Therefore, if we put $t=0$ in (23), we can describe a topographic pattern of surface or interface for each component by Fourier spectral phase, $\varphi_n(i, j)$ and amplitude $\zeta_{0n}(i, j)$ at every sampling point. If we put $t=T_n/4$, then (23) becomes

$$\zeta_n\left(i, j, \frac{T_n}{4}\right)=\zeta_{0n}(i, j)\cos\left(\varphi_n-\frac{\pi}{2}\right) \qquad \cdots\cdots\cdots\cdots\cdots\cdots (24).$$

Consequently, we will be able to compose the topographic pattern of the same component at $t=T_n/4$, from (24). In the same way, change of the spatial pattern at any time ($t=T_n/4$, $T_n/2$, $3T_n/4$, and, *e.t.c.*) in a cycle can be obtained.

The distributions of spectral phase and amplitude of the dominant components in surface and interface, and the topographic patterns of their components at $t=0$ and $t=T_n/2$ (or $t=T_n/4$ for interface), obtained in the same way as described above, are shown in Fig. 11 and in Fig. 12 respectively.

In Fig. 11, the surface seiche with the period of 4.5 hrs has only one node at the south end of the north basin, and the phase difference between the oscillation in the north basin and that in the south basin is about 180 degrees. The amplitude in the south basin is about ten times greater than that in the north basin. The oscillation of this type can be usually observed in Lake Biwa as a longitudinal uninodal seiche of the

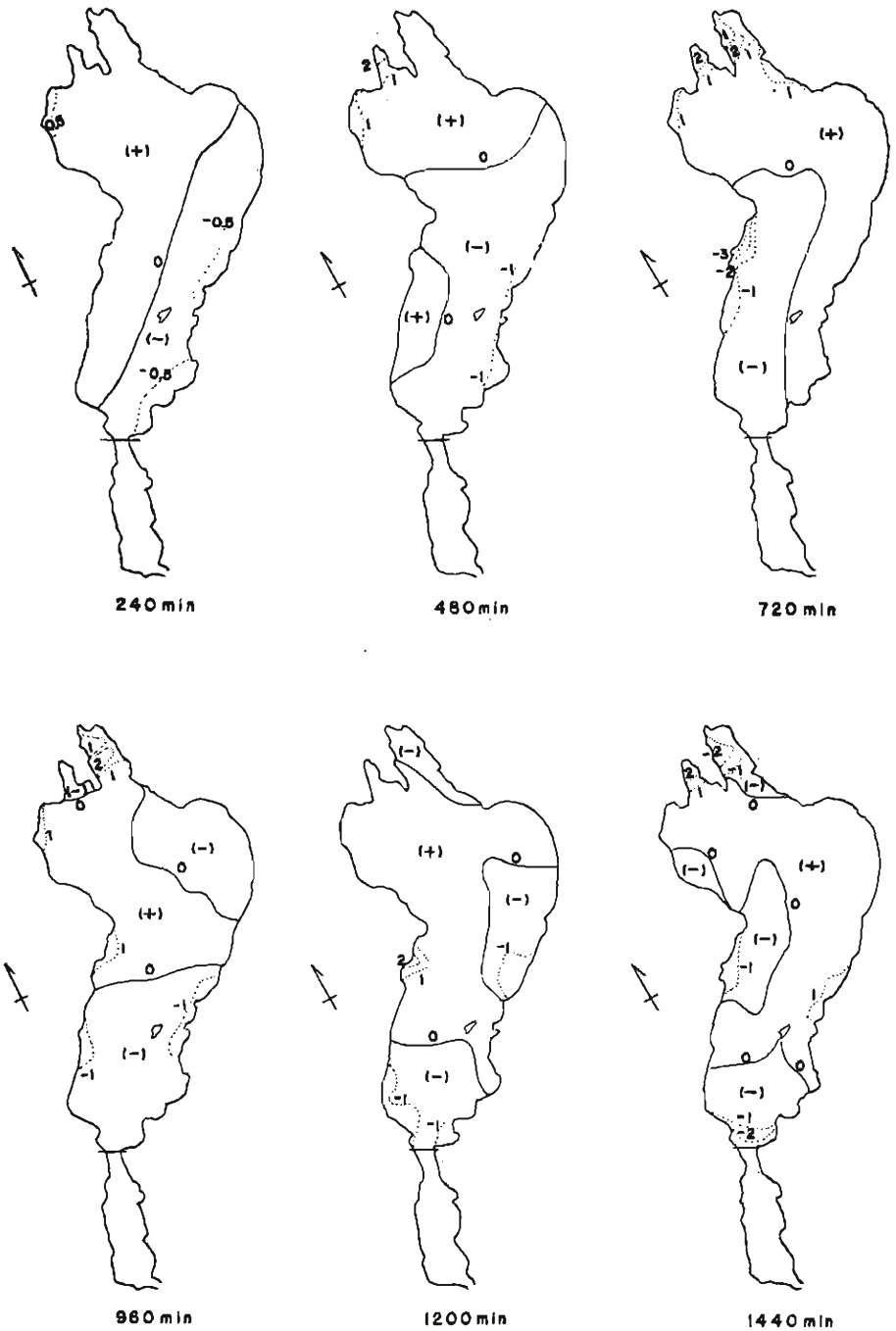


Fig. 8. Spatial elevation patterns (in meters) of the model lake interface.

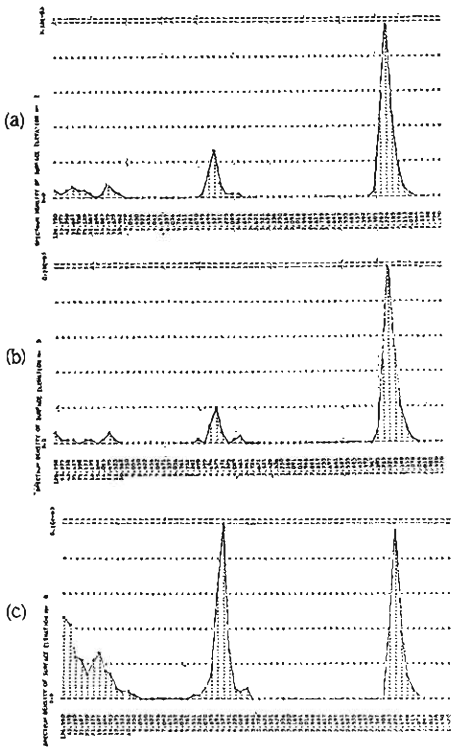


Fig. 9 (1). Power spectra of surface elevation at the sampling points of (a), (4, 24); (b), (7, 20); (c), (8, 56).

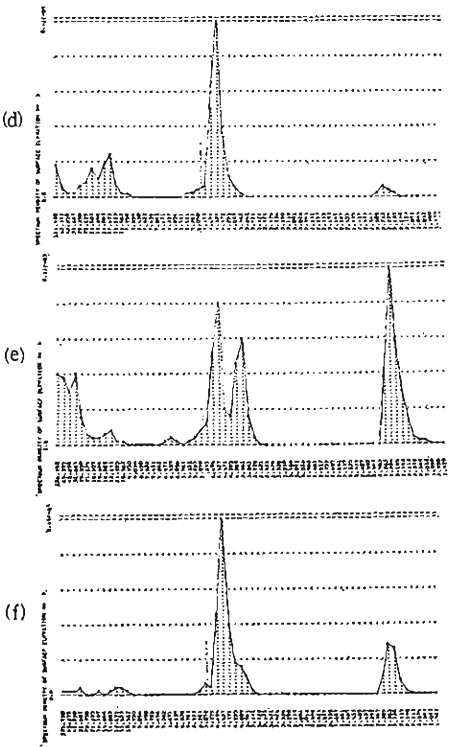


Fig. 9 (2). Power spectra of surface elevation at the sampling points of (d), (10, 40); (e), (11, 60); (f), (20, 38).

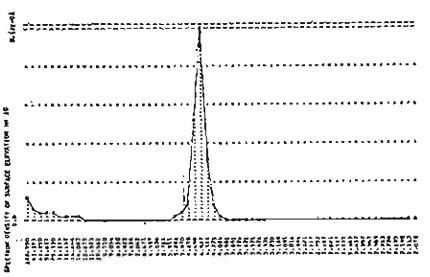


Fig. 9 (3). Power spectrum of surface elevation at the south end of the south basin (9, 3) of the model lake.

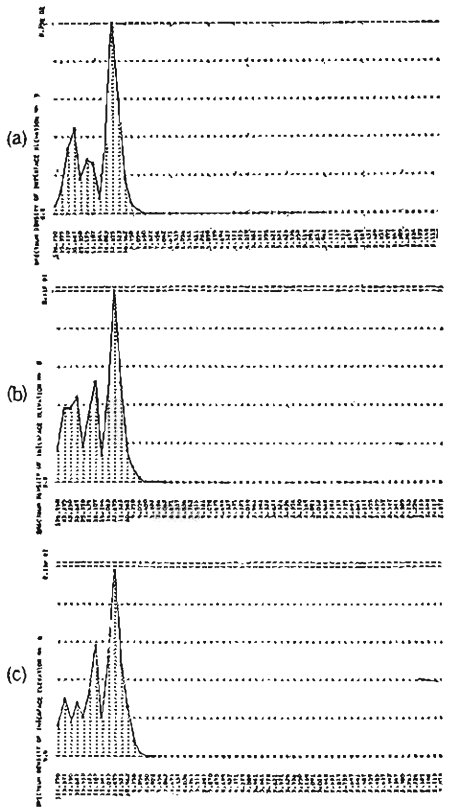


Fig. 10 (1). Power spectra of interface elevation at the sampling points of (a), (4, 24); (b), (7, 20); (c), (8, 56).

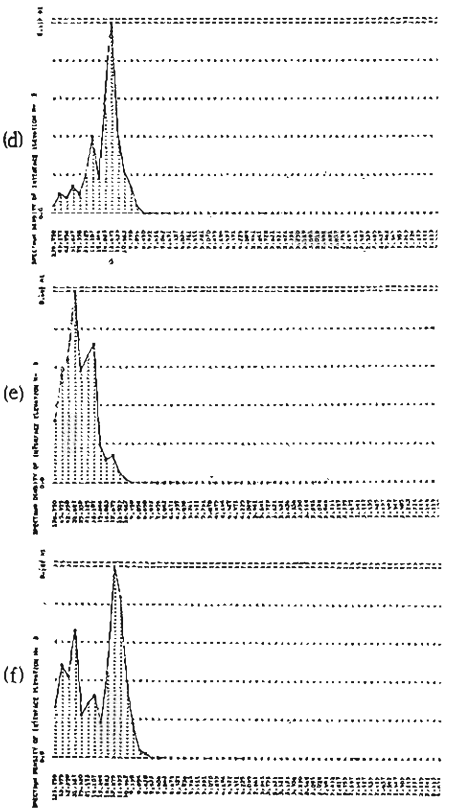


Fig. 10 (2). Power spectra of interface elevation at the sampling points of (d), (10, 40); (e), (11, 60); (f), (20, 38).

period of 4 hrs, though the estimated period in the present model is greater by 10% than observed one[11].

Another seiche as shown in Fig. 9 is also a longitudinal uninodal seiche with a period of 2.2 hrs. The nodal line lies between Kitakomatsu and Hikone, and the phase lag between the oscillations at the region of the northern part of the nodal line and at the southern part of the nodal line is also just 180 degrees, besides the amplitude in southern part of the nodal line is about three times greater than that in northern part of the nodal line. However, oscillation of this type has not yet been observed in Lake Biwa. It is to be noticed that the time interval of the time series which were expanded in Fourier series, was 45 minutes. Therefore, the period of 2.2 hrs lies near the lower limit of the period range which is thought to be able to analyze. In other words, at the range of the period of 2 hrs or so, a high resolution of the spectral analysis cannot be expected. Besides, it can be shown that the peak of the period of 2.2 hrs is due to an aliasing phenomenon. It is illustrated in Fig. 12. The thin solid line shows the calculated elevation of surface seiches at the sampling point of (4, 24), which was plotted with the time interval of 15 minutes from the line

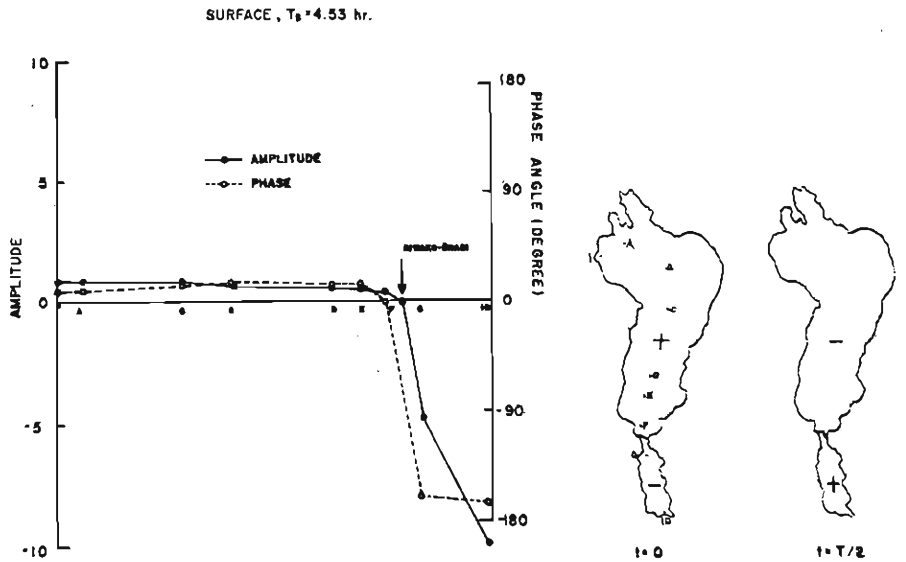


Fig. 11. Distributions of the spectral phase and the amplitude (arbitrary unit) of surface elevation along the longitudinal axis as shown with sequential points (A, B, C, e.t.c.), and the position of nodal lines at $t=0$ and $t=T_s/2$.

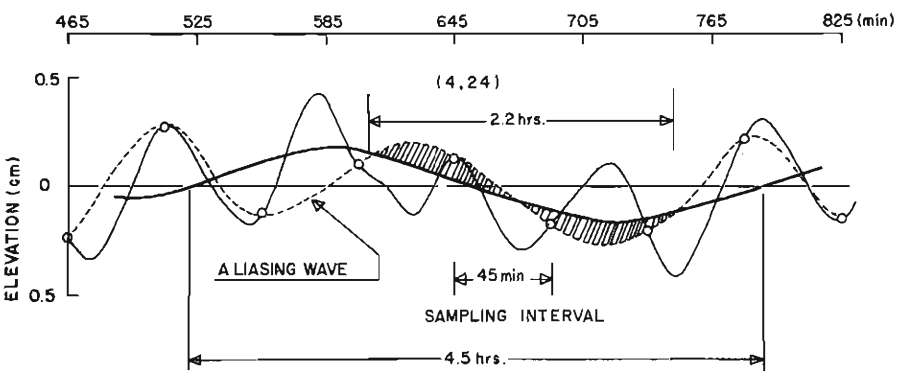


Fig. 12. An aliasing of the surface seiches.
Thin solid line, surface elevation at the sampling point of (4, 24); thick solid line, the mean variation of the sampled time series, which is the same as the mean variation of the original time series; broken line, the aliasing time series produced by rough sampling intervals of 45 minutes, which contains an illusional oscillation of the period of 2.2 hrs.

printer out-put. The elevation curve contains the short period oscillations of the period of 60 to 70 minutes rather than the longer period oscillation of the period of 4.5 hours, which is shown by a thick solid line. Oscillation of the period of 2.2 hours is evidently never contained in the original surface oscillations. However, if we take

the sample of time series with the time intervals of 45 minutes as shown by open circles, the resultant time series which is shown by broken line, does not contain the original short period oscillations, but contains the apparen oscillation of the period of 2.2 hours which was produced by rough sampling intervals.

The distribution of spectral phase and amplitude of the dominant components of interface elevation along the lake shore of the north basin and also the change of the interface topography are shown in Fig. 13. Each figure of (a), (b), (c), and (d) corresponds to the spectral components of the periods of 63.4 hrs, 31.7 hrs, 18.1 hrs, and 12.7 hrs respectively. Fig. 13 (a) shows the distribution of phase angle which varies almost linearly from 0 to 360 degrees around the lake shore, and the amplitude pattern seems to be an uninodal oscillation. However, the amplitude pattern at

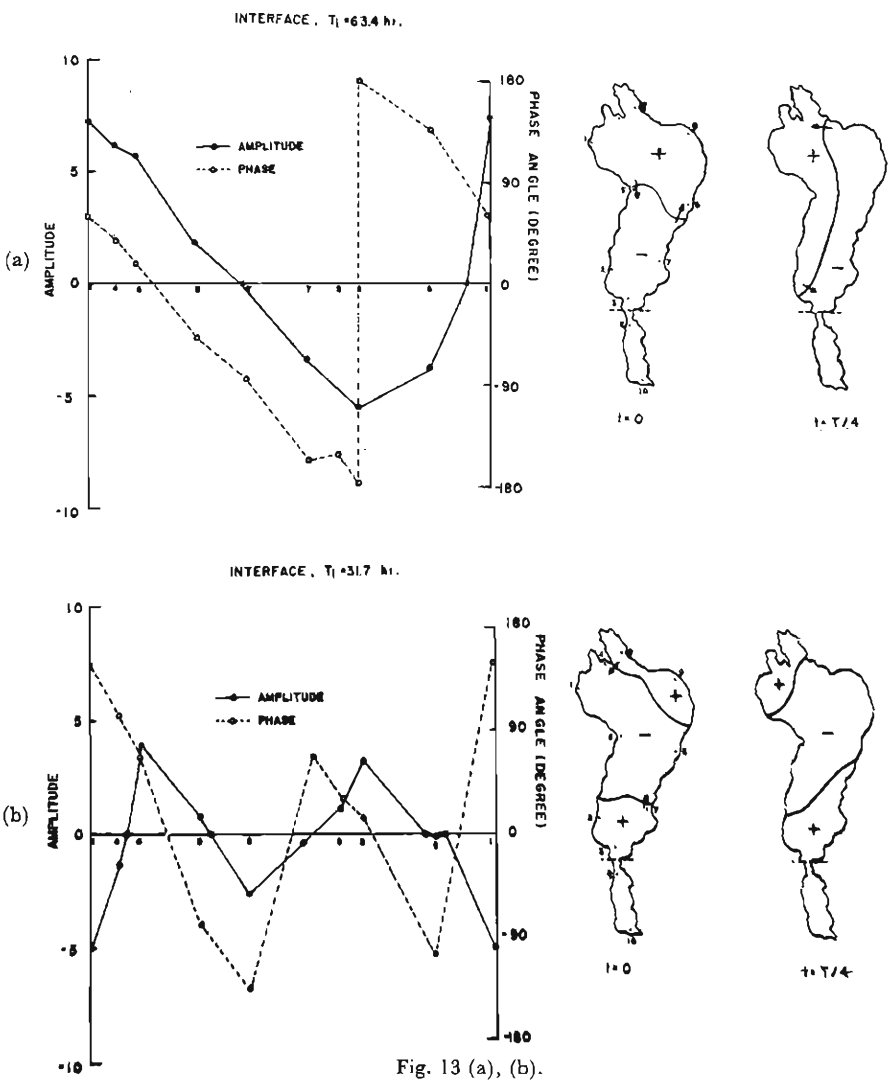


Fig. 13 (a), (b).

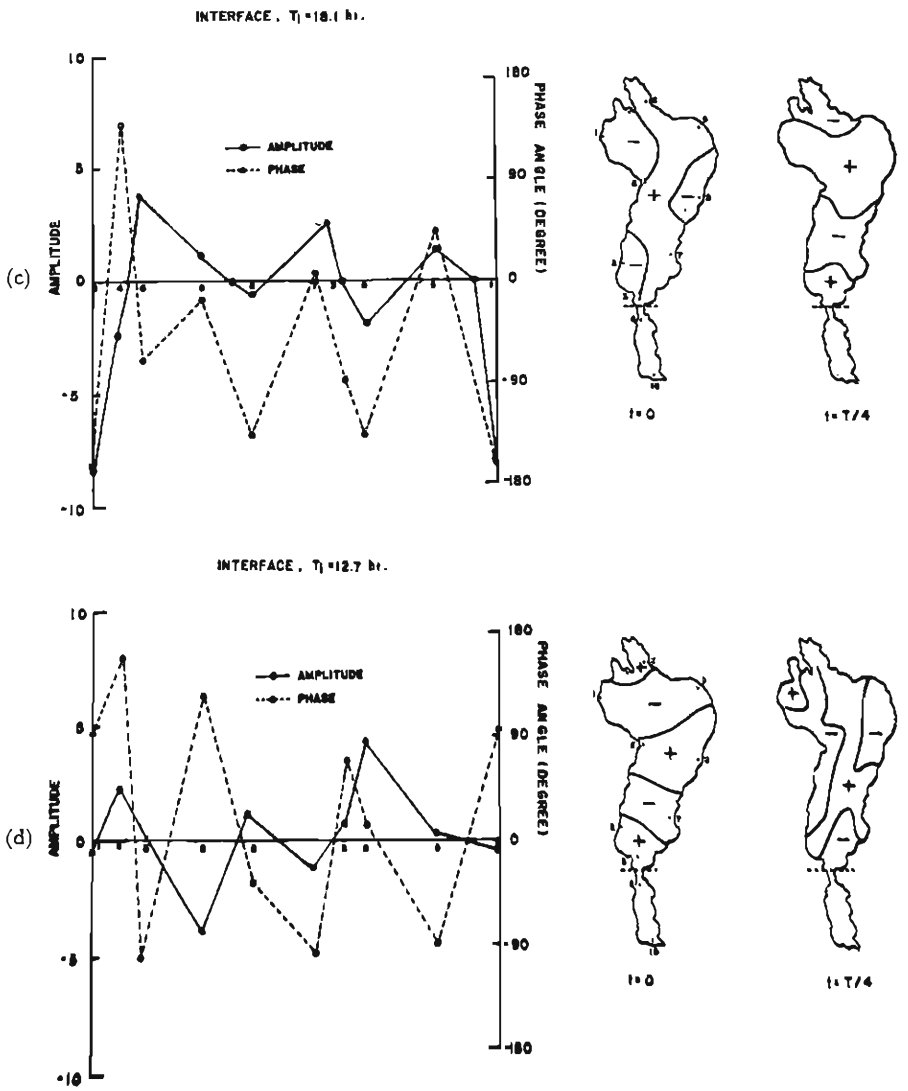


Fig. 13 (c), (d). Distributions of the spectral phase and the amplitude (arbitrary unit) of interface elevation around the lake shore of the north basin of model lake, and the position of nodal lines at $t=0$ and $t=T_4/4$.

$t=T/4$ shows that the spatial pattern is rotating in anticlockwise direction with the period of 63.4 hrs. In other words, the oscillation has an amphidromic point between Funaki-saki and Hikone. Taking the length of smoothed shore line of the north basin as 108 km, then, the apparent propagation velocity of the rotating oscillation around the lake shore is $C_p=1.7$ km/hr.

G. T. Csanady (1967)[2], and G. E. Birchfield (1969)[3] have treated the two layer problem for the circular Great Lake model, and showed that the long period internal Kelvin wave in the circular lake always has an apparent propagation velocity close to the velocity $C_2$ which would be the wave propagation velocity in the absence of

rotation.

In the present case, the wave propagation velocity without rotation becomes

$$C_2=\sqrt{\Delta\rho g h_1 h_2/\rho(h_1+h_2)}=1.9 \text{ km/hr}$$

$$(=53 \text{ cm/sec}),$$

Therefore, the ratio of $C_p$ and $C_2$ becomes nearly equal to unity.

According to Birchfield, more detailed characteristics of the longest period internal Kelvin wave in the circular basin are that the initially horizontal interface is elevated on the left side of the basin and depressed on the right side of the basin, facing downwind. With the rise, the cotidal lines shift very slowly in a counterclockwise direction. The point of maximum displacements are confined to within a short distance from the coast.

A longitudinal section of interface elevation pattern of the present model along the line which is in right-angle to the initial nodal line, is shown in Fig. 14. The longitudinal section of the elevation pattern containing the exponential increase (or decrease) of elevation at the coastal region, and showing a rise on the left side (facing downwind) and a depression on the right side of the basin. Of course, the pattern rotates in anticlockwise direction with the nodal line. These features just coincide to those which were summarized by Csanady[2] and also Birchfield[3]. Consequently, the rotating pattern shown in Fig. 13 (a) are concluded to be the longest period Kelvin waves in Lake Biwa.

The oscillation shown in Fig. 13 (b) also has the same behavior as that mentioned above, though it has two nodal lines.

Now, we will apply the circular basin analogy to the present model, then the criterion of the possible internal Kelvin modes is stated as the following inequality;

$$\left(\frac{r_e}{R_2}\right)^2 > k(k+1) \qquad \cdots\cdots (25),$$

where, $r_e$ is the equivalent radius of the lake, and $R_2$ is the Rossby's "radius of deformation" for the internal mode which is characterized by

$$R_2=C_2/f \qquad \cdots\cdots (26),$$

and $k$ is the azimuthal wave number and takes positive integers. For the present model, $(r_e/R_2)^2$ takes the value of 4.9, therefore, the inequality of (25) can be satisfied by $k=1$ only.

If we apply the criterion to the surface mode, then, $(r_e/R_1)^2$ becomes 0.00023, and therefore, there is no Kelvin wave in the surface mode. The long period Kelvin waves as seen in surface spectra with a small fraction are not the Kelvin waves of the surface mode, but a small contribution of the Kelvin waves of internal mode.

As mentioned above, if we apply the circular basin analogy to Lake Biwa, then, the internal Kelvin waves will be permissible only for $k=1$. However, the oscillation of 31.7 hrs period which has two nodal lines, is showing anticlockwise rotation. It seems that the oscillation of 31.7 hrs period is the second mode Kelvin wave for $k=2$, and therefore, the criterion of the long period Kelvin waves as discussed above must be taken with some adjustment for Lake Biwa.

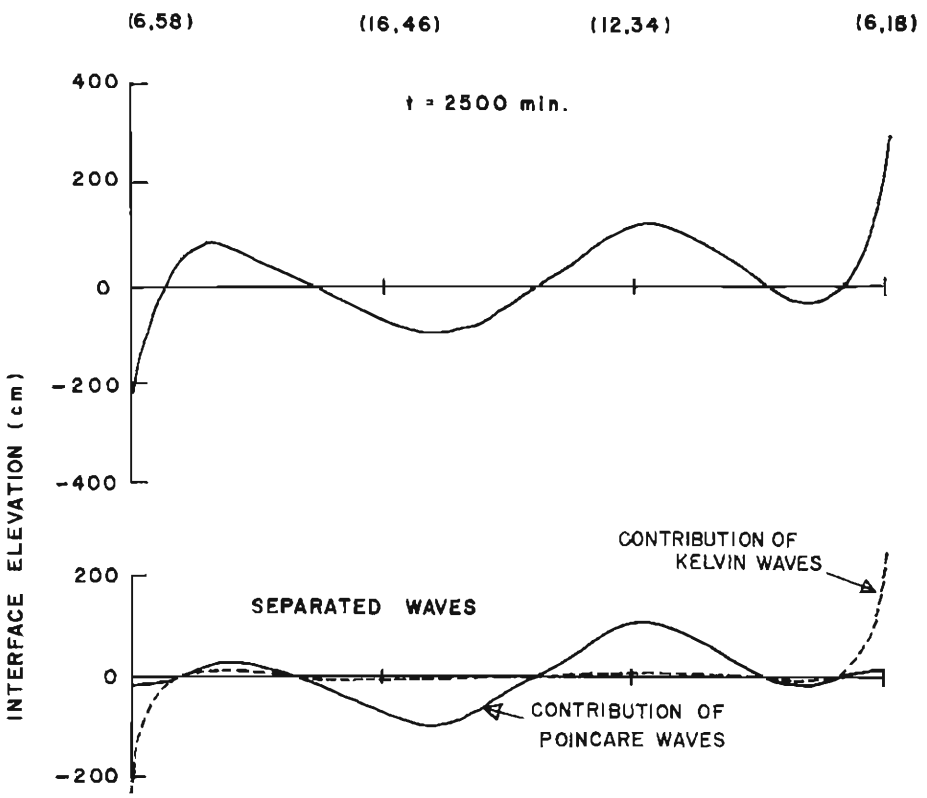


Fig. 14. Cross-sectional interface elevation pattern at $t = 2500$ min. The broken line shows the contribution of the longest period Kelvin wave, which was separated from the original elevation pattern shown in upper panel by multiplying the factor of exp $(-\mu x)$, $\mu = f/C_2$. The solid line in the lower panel shows the residue of subtraction of the Kelvin wave contribution from the original elevation pattern.

The other oscillations as shown in the figures (c) and (d) also showing the rotatory natures, though they have more than two moving nodal lines and rotate partly in clockwise direction. Their rotation is not so clear, because of the composition of clockwise and anticlockwise rotations with variable amplitudes. They have periods slightly shorter than the inertial period. Besides, as shown in Fig. 14, their distribution of amplitudes along the longitudinal direction are larger in the inner part of the lake rather than near the shore. Consequently, these oscillations may be the higher modes Poincare waves.

Fig. 15 shows some examples of magnitudes of the spectral power of the surface oscillations and the internal oscillations. From the figure, it is seen that the ratio of the spectral amplitudes between surface and interface elevations are in the order of $10^{-2}$ in the range of the long period internal waves and in the order of $10^{-3}$ in the range of the period of surface seiches.

In the same figure, the power spectra of the case of twenty hours of wind blowing are also shown as model-L7. From the comparison between the power spectra of

the present model (model–L6) and of the other model (model–L7), it is seen that the maximum peak of the model–L7 is shifted to the period of the longest Kelvin wave (63 hrs), while the maximum peak of the present model is near the inertial period. Such a tendency may be suggests that the oscillations in the longer period range may resonate with wind, depending on the length of wind blow, and the length of wind blow may determine the prevailing period of internal waves.

The characteristics of various oscillations discussed above are all tabulated in Table 1.

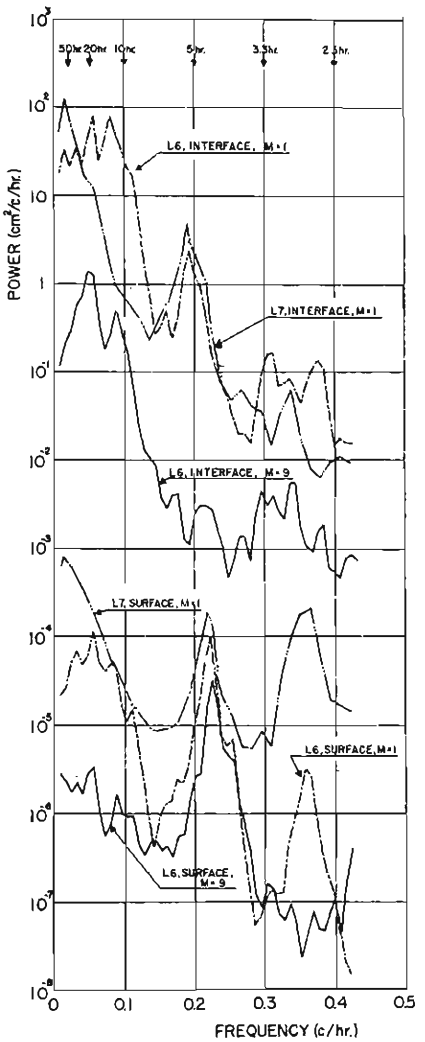


Fig. 15. Some examples of power spectrum of surface and interface elevations in logarithmic scale. The solid line and the single dotted line show the power spectra of the present model at the points of (2, 52) and (22, 50) respectively. The double dotted line show the power spectra of another model, in which wind blow was continued for twenty hours.

Table 1. Characteristics of Oscillations.

| Length of wind blow | Layer | Period (hrs) | Power ($cm^2/c/hr$) | Wave length (km) | Wave Velocity (km/hr) | Wave numbers | Remarks |
|---|---|---|---|---|---|---|---|
| 7.5 hrs. | Surface | 63.4* | $9.6\times10^{-4}$ | 108 length | 1.7 (apparent) | 1 | Rotatory, anticlockwise. |
| | | 4.5 | $1.3\times10^{-2}$ | 120 | 26.7 | 1 | Ordinary seiche, uninodal. |
| | Interface | 63.4 | $3.3\times10$ | 108 | 1.7 (apparent) | 1 | Rotatory, anticlockwise. |
| | | 31.7 | $3.5\times10$ | 54 | 1.7 (apparent) | 2 | Internal Kelvin waves. |
| | | 18.1 | $8.0\times10$ | 36 | 1.7 (apparent) | 3 | Rotatory, clockwise and anti-clockwise, partly. |
| | | 12.7 | $7.9\times10$ | 27 | 1.7 (apparent) | 4 | Internal Poincare waves. |

* This oscillation is one of the Internal Kelvin modes appeared in surface.

(d) Pattern of lake currents.

Pattern of wind driven lake currents at the final stage of wind blow are shown in Fig. 16. In the upper layer (titled as layer-1), high velocities appear at the south

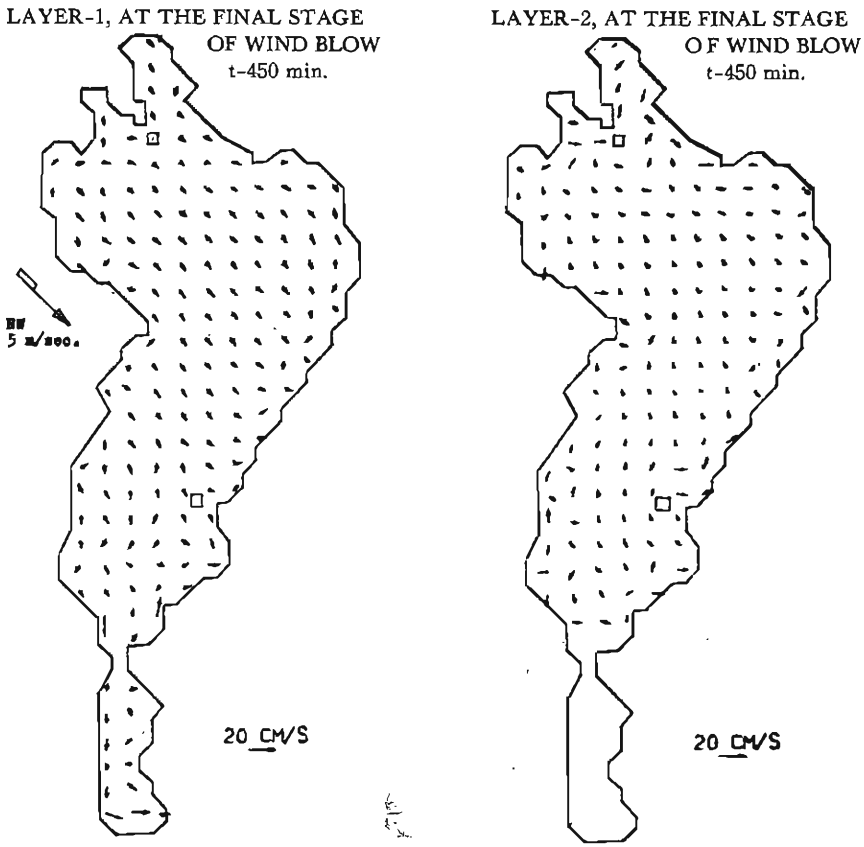


Fig. 16. Horizontal velocities at the final stage of wind blow.

end of the north basin and at the south end of the south basin. A weak anticlockwise gyle is seen at the south end of the south basin, however, almost all current vectors are directed towards south or south-east. In the lower layer (layer-2), two small scale anticlockwise gyles appear in southern part of the north basin.

Fig. 17 and Fig. 18 also show the patterns of current vectors in both upper and lower layers at 4800 minutes and at 6000 minutes after falling down of wind. In these figures, large scale, but weak circulation patterns are also recognized, however, it is to be noted that the direction of the circulating currents cannot be unchanged. For an example, at the north-western part of the north basin, the circulation of the upper-layer is clockwise at a time of 4800 min after the falling down of wind, but this circulation has turned to an anticlockwise one at a time of 6000 min. These slow variations of the current patterns will be due to a large scale quasistatic motion as the longest Kelvin wave, superposed by the internal Poincare waves. Concerning

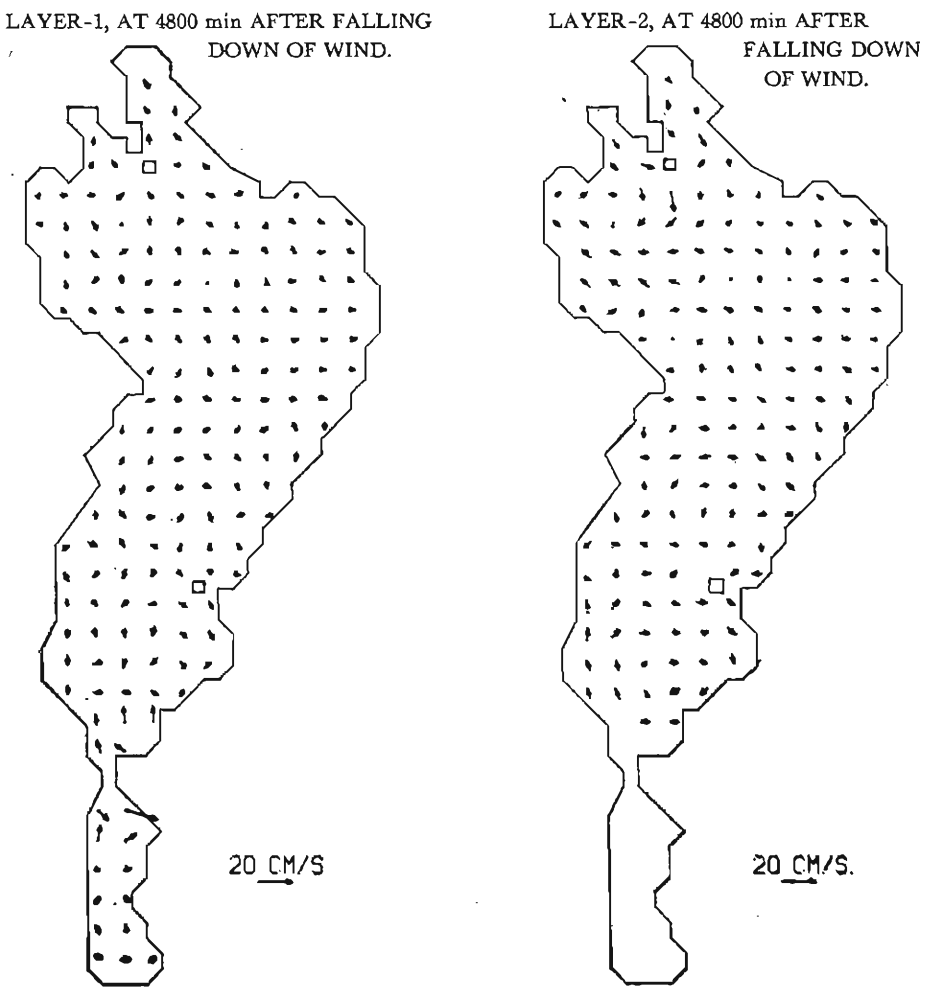


Fig. 17. Horizontal velocities at 4800 minutes after falling down of wind.

to the current system, many investigators still now be entertaining an opinion of the existence of the everlasting three strong gyles in Lake Biwa, as was insisted by early investigators. However, it is not the usual pattern, but some stage of the current system which is slowly changing as the quasi-static motions.

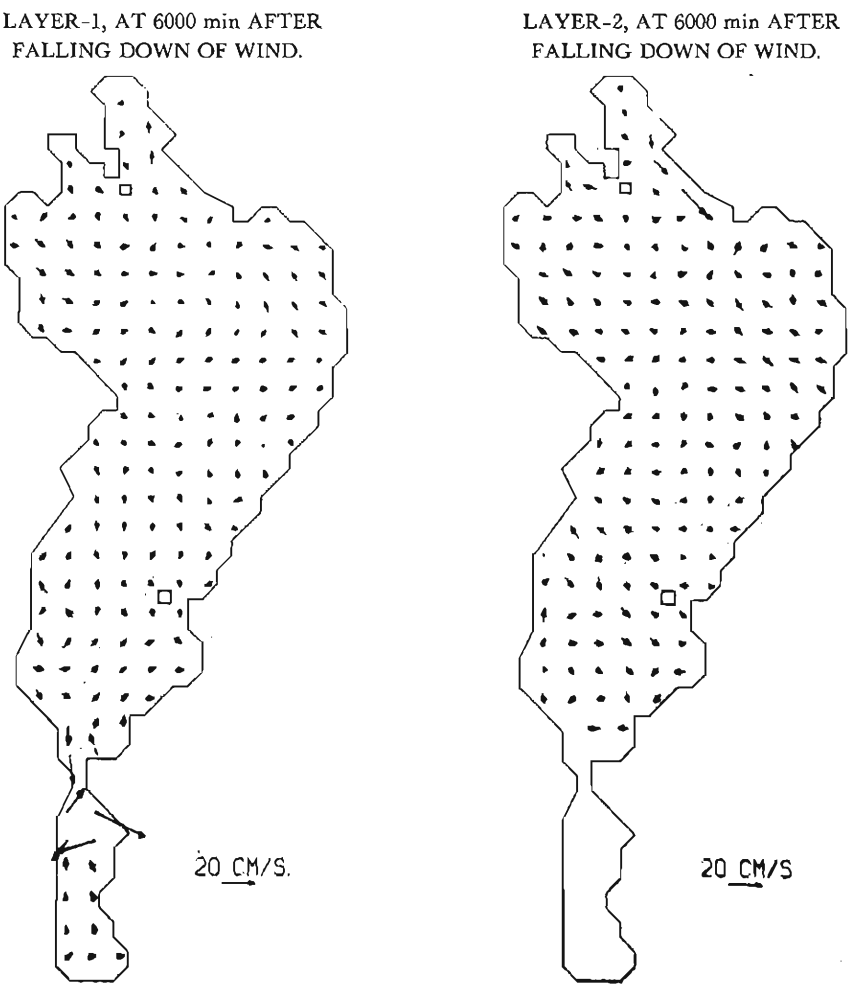


Fig. 18. Horizontal velocities at 6000 minutes after falling down of wind.

## 7. Conclusion.

In the present paper, response of the two layer model Lake Biwa to a suddenly imposed NW-wind of 5 m/sec was treated. The obtained results are as follows;

(1) The setup of the new equilibrium water surface is accomplished about 1.2 hrs after wind rises. During wind blow, the water surface oscillates around the tilted equilibrium surface, but after the blowing down of the wind, it oscillates freely as surface seiches around the horizontal equilibrium surface.

(2) The surface seiche with the period of 4.5 hrs is prevailing as the uninodal seiche. The nodal line appears at the south end of the north basin and maximum amplitude occurs at south end of the south basin. Another maximum amplitude occurs at north end of the north basin but its magnitude is less than one-tenth that of the south basin.

The other surface seiche with the period of 2.2 hrs is also prevailing as the uninodal longitudinal seiche. The nodal line appears at the middle part of the north basin. However, the seiche has been never observed in real Lake Biwa. Consequently, it is supposed that the seiche might be due to an aliasing effect.

(3) In the spectra of the interface elevation, the dominant peaks are at 18.1 hrs and 12.7 hrs. Other comparable peaks also appeared at the periods of 31.7 hrs and 63.4 hrs. The oscillation of the period of 63.4 hrs having a nodal line initially parallel to the wind direction and the elevation pattern rotates in the anticlockwise direction around the lake shore with the apparent propagation velocity of 1.7 km/hr, which is very close to that in the Great Lake model (the apparent velocity is 1.6 km/hr in the Great Lake). From the analogy of a circular model basin, the rotating oscillation was classified as the longest period Kelvin wave. But, the analogy of a circular model basin cannot be applied to the higher modes of Kelvin waves, because the centers of the respective rotating nodal lines of higher mode Kelvin waves appeared at different positions in the present model, while the center of rotating nodal lines appeared at the same position which is the center of the circular basin.

The oscillation of the period of 31.7 hrs has the nature of anticlockwise rotation, though it has two nodal lines. Also, this oscillation may be the second mode of the internal Kelvin waves in the present model lake.

The other two oscillations have three or four nodal lines and their spatial patterns also rotate anticlockwise, but also partly clockwise direction with respective periods which are close to the inertial period. These may be classified as the baroclinic Poincare waves, however, more detailed analysis will be needed for this point.

(4) Local weak gyles appeared in the current system of both upper and lower layers. However, they seem to be changeable depending on the quasistatic oscillations.

(5) As presented in the experiments, the maximum spectral amplitude appeared at the period of 18.1 hrs. But, in the other model of the duration time of twenty hours of wind, the maximum amplitude occurs at the period of 63 hrs of the longest period Kelvin mode as shown in Fig. 15.

The problem of the existence of the rotating internal seiches, especially of the long period Kelvin waves, is the main topic of the present paper. The experimental results show the existence of such rotatory seiches also in Lake Biwa, though it is not yet confirmed in the real Lake Biwa. However, as mentioned in section 1, the observed results at Funaki-saki (Fig. 19) seems to support the experimental results. Of course, concerning to the point, the direct confirmation through a high speed cruising survey is now under consideration.

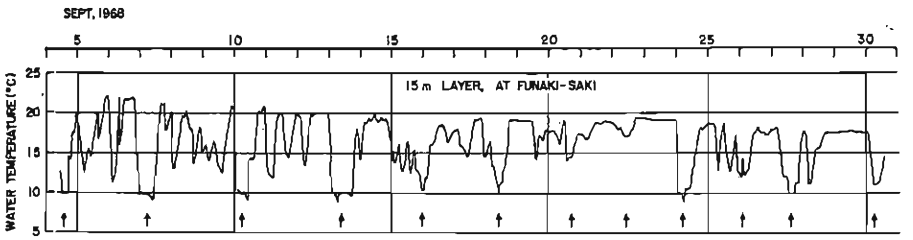


Fig. 19. Recorded temperature oscillations of 15 meter-layer obtained by thermister buoy station at 200 meters off the shore of Funaki-saki. The arrows show the maximum elevation of the top of hypolimnion. The mean interval of adjoining arrows is 56.7 hrs which corresponds to the period of internal seiche in this season. The amplitudes of the temperature variations are not less than that observed at the both end of the north basin of Lake Biwa.

## Acknowledgements

The author wishes to express his sincere appreciation to Professors H. Kunishi and S. Okuda of Kyoto University. The study was partly supported by the Science Research Fund of the Ministry of Education and thanks are due to the Ministry for this. The numerical computation was made by the use of the computer of the Data Processing Center of Kyoto University.

## References

1) Kanari, S., Internal waves in Lake Biwa (I) — The responses of the thermo cline to the wind action —, Bulletin of the Disaster Prevention research Institute, Kyoto University, Vol. 19, February 1970, pp. 19–26.
2) Csanady, G. T., Large-scale motion in the Great Lakes, J. G. R., Vol. 72, No. 16, 1967, pp. 4151–4162.
3) Birchfield, G. E., Response of a circular model Great Lake to a suddenly imposed wind stress, J. G. R., Vol. 74, No. 23, 1969, pp. 5547–5554.
4) Veronis, G., Partition of energy between geostrophic and non-geostrophic oceanic motions, Deep Sea Res., 3, 1956, pp. 157–177.
5) Charney, J. G., The generation of oceanic currents by wind, J. Marine Res., Vol. 14, 1955, pp. 477–498.
6) Kunishi, H., Studies on wind waves by wind flume experiments (II) — On the Generation and growth of wind waves—, J. Oceanogr Soc. Japan, 20th Anniversary Volume, 1962, pp. 470–486.
7) Reid, R. O., Modification for the quadratic bottom-stress law for turbulent channel flow in the presence of surface wind stress, Tech. Mem. Beach Erosion Board, No. 93.
8) Miyazaki, M., Destructive waves caused by heavy storms in Osaka Bay, Ocean. Rept. CMO, 2 (2).
9) Nakano, M., On the decay of the seiche motions in Lakes (in Japanese), Preliminary Abstract, Limnol. Soc. Japan, 1971, pp. 145–146.
10) Kasahara, A., On certain finite-difference methods for fluid dynamics, monthly Weather Review, Vol. 93, No. 1, 1965, pp. 27–31.
11) Imasato, N., Study of seiche in Lake Biwa-Ko (I) — On the numerical calculation by Defants method —, Spec. Contr. Geophys. Inst. Kyoto Univ., No. 10, 1970, pp. 93–103.